Review

Fully Hydrogenated and Fluorinated Bigraphenes–Diamanes: Theoretical and Experimental Studies

Leonid A. Chernozatonskii *, Victor A. Demin and Dmitry G. Kvashnin

Emanuel Institute of Biochemical Physics, Russian Academy of Sciences, 4 Kosigin St., 119334 Moscow, Russia; victordemin88@gmail.com (V.A.D.); dgkvashnin@gmail.com (D.G.K.)
* Correspondence: chernol-43@mail.ru

Abstract: Diamanes are 2D diamond-like films that are nanometers in thickness. Diamanes can exist as bilayer or multilayer graphene with various modes of stacking and interlayer covalent sp^3 bonds. The term "diamane" is used broadly for a variety of diamond-like materials at the nanoscale, from individual diamond clusters to nanocrystal films. A short overview of recent progress in the investigation of diamanes, starting from the first theoretical predictions to practical realization, is presented. The results of both theoretical and experimental studies on diamanes with various atomic structures and types of functionalization are considered. It is shown that diamanes are stronger than graphene and graphane and have wide bandgaps ranging from 3.1 to 4.5 eV depending on the structure. Diamane-like structures have been obtained using different experimental techniques, and their structures have been determined by Raman spectroscopy. The potential applications of these carbon nanostructures are briefly reviewed.

Keywords: 2D diamond; diamane; Moiré structure; electronic properties; mechanical properties; Raman spectra

1. Introduction

The discovery of graphene in 2004 [1] drew enormous attention from researchers studying two-dimensional (2D) structures, which has been maintained over the last 15 years [2]. In 2009 [3], a new 2D material based on AA- or more stable AB-stacking bilayered graphene with interlayer covalent bonds was predicted and studied. This sp^3-carbon dielectric material can be formed after the hydrogenation of bigraphene surfaces and was named "diamane" (Dn) in analogy to "graphene–graphane" [4] (Figure 1). Fluorinated diamanes (F-Dn) were described later [5,6]. The stability of most predicted diamane structures is achieved by the functionalization of both surfaces. Among the diamane, a structure with only one functionalized surface was also predicted, while an opposite surface was represented as an array of dangling bonds; this unique structure was called "diamondene" [7]. The unique properties of predicted and experimentally synthesized 2D diamonds—such as the high thermal conductivity [8–13], high hardness [3,14,15], excellent properties for electromechanical vibrators [12], optic peculiarities [16–18], and wide-gap spectra with many resonance peaks in valent and conductive bands in the density of states [17,18]—make such structures promising candidates for the main components in future nanoelectronics, optics and photonics.

Diamane-like structures represent a new class of 2D materials. Many newly published studies devoted to the synthesis and investigation of the thinnest-possible diamond films are discussed in the present review.

1.1. Fully Hydrogenated and Semi-Hydrogenated Bilayer Graphenes—Theoretical Studies

The atomic and electronic structure of single-layer diamanes compared with those of graphene, as observed by various research groups, are discussed here.
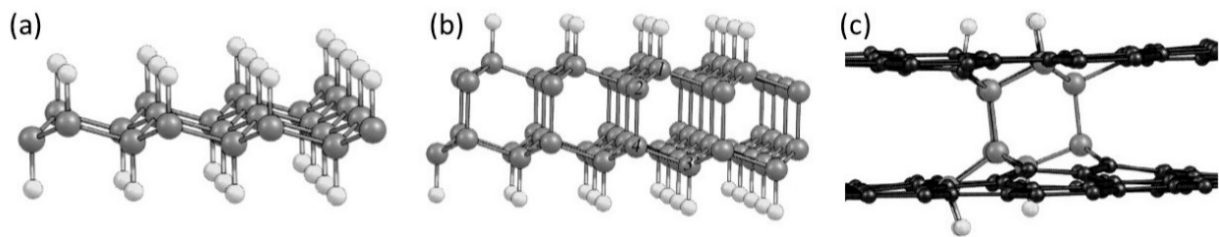
Figure 1. Atomic structures of (**a**) graphane and (**b**) diamane, and (**c**) the mechanism of the diamane nucleus formation on the initial graphene bilayer: hydrogen atoms are attached on two sides and initiate the "adhesion" of carbon atoms over each other in neighboring layers organized with AB (Bernal) stacking. The carbon and hydrogen atoms are shown in dark and bright gray, respectively. Black circles in (**c**) correspond to sp^2 carbon atoms.

The energy stability, electronic and phononic properties of these ultrathin sp^3-bonded carbon films have been predicted by density functional theory (DFT) using the Vienna Ab initio Simulation package (VASP) [19]. Diamane is more stable than graphene (its formation energy is −0.03 eV/atom lower than formation energy of graphene) and has a direct dielectric bandgap (E_g) of 3.12 eV (Figure 2a) in its band structure, in contrast to graphene. Its stiffness coefficient was estimated from the molecular dynamic modeling of its membrane deformation (Figure 2c,d); diamane is stronger than graphene and graphane, according to the estimated elastic constants of 238, 449 and 715 N/m, respectively [3,20,21]. Diamanes are very similar in their properties (geometric structure and mechanic and electronic properties) to diamond crystals [3,20,21].
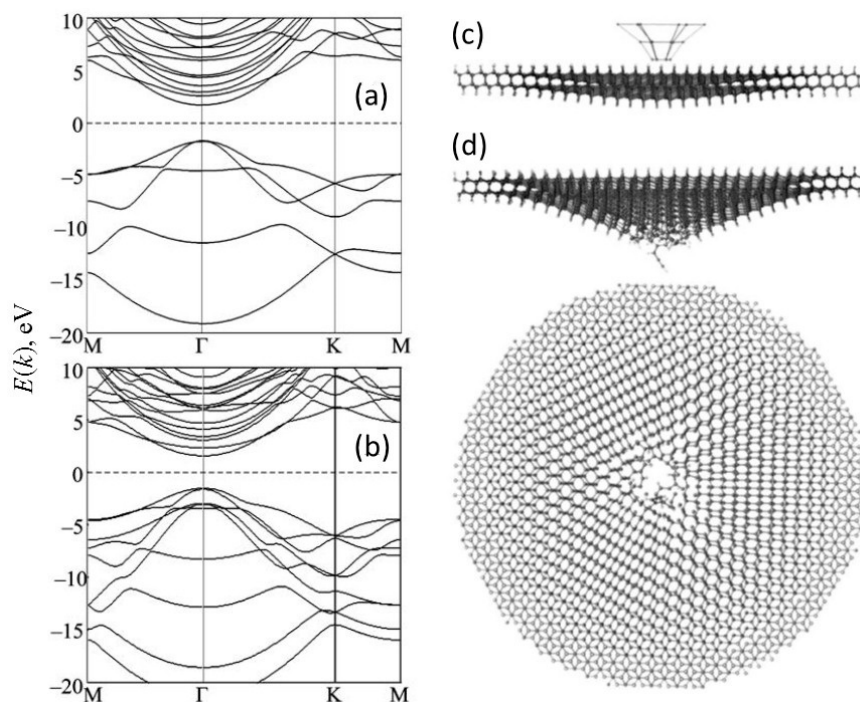

Figure 2. Band structures of (**a**) graphane, CH, and (**b**) diamane, C_2H, (the Fermi level is taken as zero) and the dynamics of the diamane membrane's deformation; (**c**) elastically deformed structure and (**d**) membrane break.

Diamanes are potentially very interesting for electronics and electromechanical microsystems, and the direct energy gap of diamane can be harnessed for nanophotonics. O. Leenaerts et al. [22] studied the hydrogenation of a graphene bilayer and obtained similar results for it through ab initio calculations (excluding for the mechanical properties).

Almost simultaneously, the first derivative of diamanes was studied by D.K. Samarakoon and X.-Q. Wang [23], who proposed and calculated a semi-hydrogenated graphene bilayer in an ordinary "chair" (AB-stacked bigraphene) conformation and "boat" H-C-C-H

configuration, 2D lonsdaleite (Dn-L) (Figure 3). The forerunner of these structures was one-side hydrogenated graphene [24], later named "graphone" [25]. Thus, the semi-hydrogenated graphene bilayers can be called "diamones" (Dons) because they are based on "diamandols" [26] transformed from a few graphene layers covered by molecules on only one side. The binding energy (E_B), bandgap (E_g) and interlayer bond length (L) for Dn and Dn-L structures, and also for Don-L (semi-hydrogenated "boat I" with interlayer bonding) and a graphone boat on graphene (semi-hydrogenated "boat II" without interlayer bonding), were calculated (Table 1).
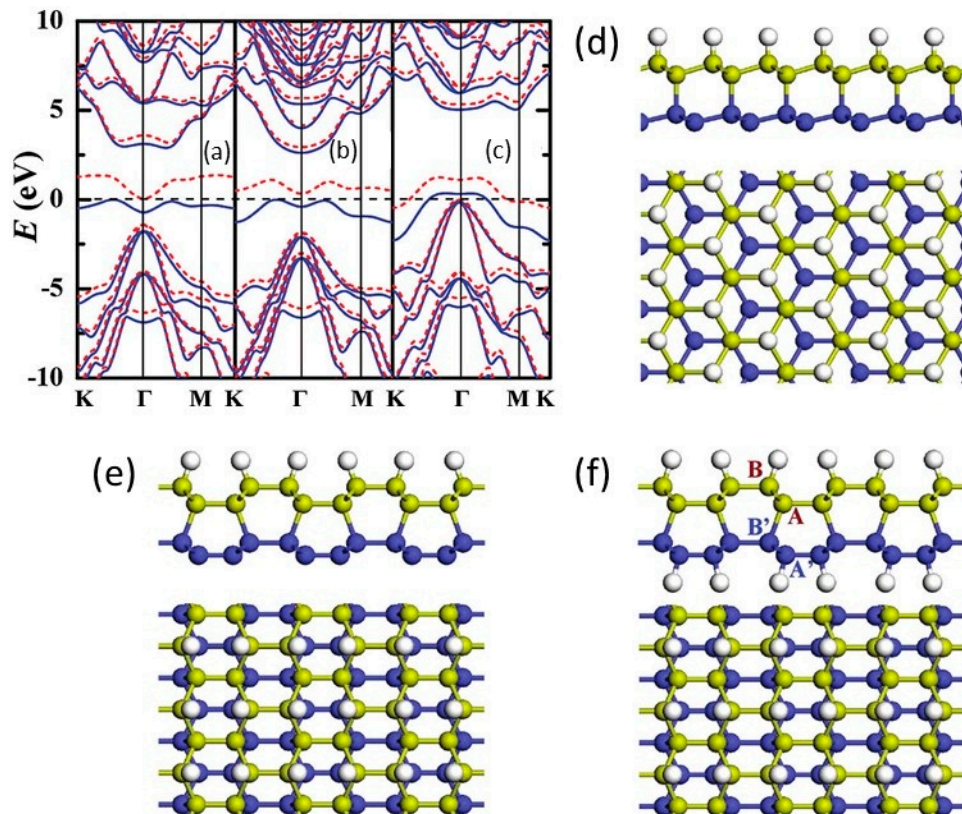
Figure 3. Band structures (**a**–**c**) of semi-hydrogenated diamane (Don) with lonsdaleite structure (**d**), later named "diamone" [21], with normally applied electric field E: (**a**) −0.26 V/Å, (**b**) no electric bias and (**c**) 0.39 V/Å (the red and blue curves represent spin-up and spin-down components); semi-hydrogenated diamane Don-L (**e**) and fully hydrogenated diamane Dn-L (**f**) with "boat" structures. C atoms on the top and bottom layers are gold and blue balls, respectively. H atoms are white balls [23].

The semi-hydrogenated structure arising with a periodic array of dangling bonds on the bottom layer was characterized as a 2D ferromagnetic semiconductor with spin-polarized bands (Figure 3a), marking it as a promising candidate for spintronics.

When an external electric field was applied normal to the Dn and Don surfaces, the Dn bandgap decreased monotonically with an increase in the electric field from 3.2 to 0 eV. This shows the continuous tuning of the bandgap as Dn transitioned from a semiconducting to metallic state. The critical electric field value for this transition was estimated to be 1.05 V/Å. The magnetic Don structure, which could be formed by the desorption of hydrogen atoms from one of the surfaces in the chair conformation, had a ferromagnetic semiconducting nature with a non-monotonic dependence of the bandgap on the electric field value (Figure 3a,b). The implications of tailoring the band structures of biased systems for future graphene-based devices were discussed. Thus, along with AB diamane, stable forms of other diamane-like structures may exist.

Table 1. Estimated binding energy per carbon atom (E_B), bandgap (E_g) and interlayer bond length (L) for chair and boat conformations of fully hydrogenated and semi-hydrogenated graphene, respectively [23]. Labels I and II refer to boat conformations with and without interlayer bonding, respectively.

| Structure	E_B (eV)	E_g (eV)	L (Å)
Fully hydrogenated chair	−12.00	3.24	1.54
Fully hydrogenated boat	−11.93	2.92	1.54
Semi-hydrogenated chair	−10.55	0.54	1.65
Semi-hydrogenated boat I	−10.79	2.35	1.63
Semi-hydrogenated boat II	−10.85	0.50	3.26

We sought studies on fluorinated graphite and found experiments conducted in the 1980s where the electron microscopy of unknown three-dimensional inclusions in the material showed structures with an interlayer distance of 1.0–1.2 nm [27]. They were interpreted as a stack of C_2F layers, which was substantiated by the presence of only sp3-hybridized bonds between the carbon atoms and between the carbon and fluorine atoms. A subsequent study in 1987 [28] proposed an atomic model to explain the experiments: a CF_2 structure based on AB and AA′ graphite layers (see Figure 4), corresponding to the diamond and lonsdaleite structures. Notably, these structures are essentially atomic ones of diamanes; the case is similar to the comparison of graphene and graphite structures, when the description and calculation of a single layer of graphite were documented in 1947 by P.R. Wallace [29].
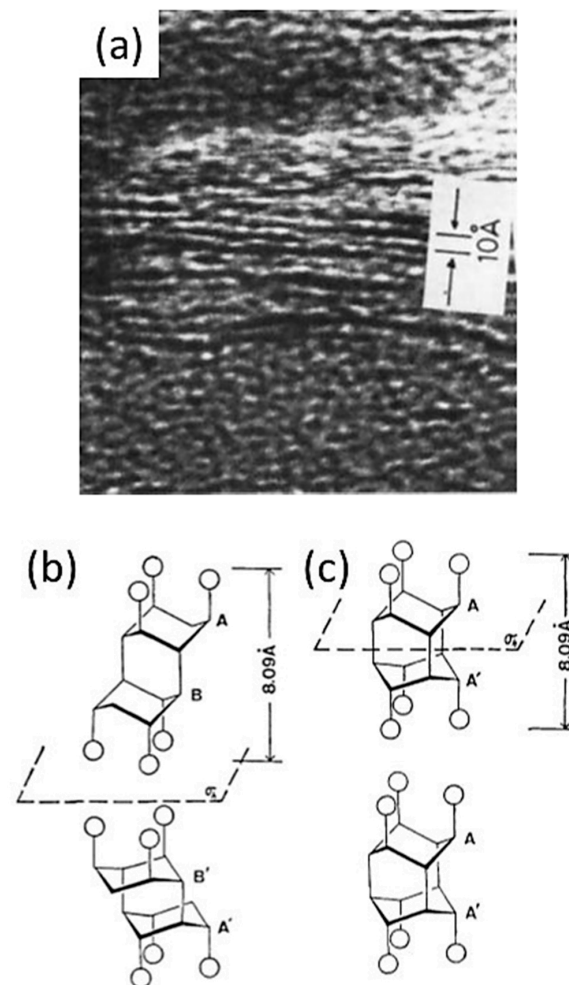
Figure 4. Scanning electron micrograph of $(C_2F)_n$ (**a**) and structural models for stacking patterns of carbon difluoride in adjacent layers AB/B′A′ (**b**) and AA′/AA′ (**c**) (σ_h is a mirror plane perpendicular to the principal symmetry axis) [28].

1.2. Experimental Evidence of the First Representative of 2D Diamond-Like Structures

Barboza et al. [26] proposed and conducted experiments supporting the existence of a Dn-derivative material—2D diamonds in which only one surface of the multilayer graphene was covered by hydroxyl groups, synthesized by a room-temperature compression method. This diamond structure, semi-covered by hydroxyl groups, named "diamondol", was transformed from multilayer graphene and had a structure and properties very similar to those of "diamone" [23]. The authors [26] characterized this material as a 2D ferromagnetic semiconductor with spin-polarized bands. These unique properties, which arise from the periodic array of dangling bonds on the bottom layer, make this material a promising candidate for spintronics. The observed compression-induced charging inhibition of bilayer and multilayer graphene is reversible and is absent in single-layer graphene. Based on ab initio calculations, the authors showed the spontaneous diamondization of few-layer graphene by hydroxyl functionalization. The obtained structure has a ferromagnetic insulator phase with different bandgap energies for each spin (Figure 5).
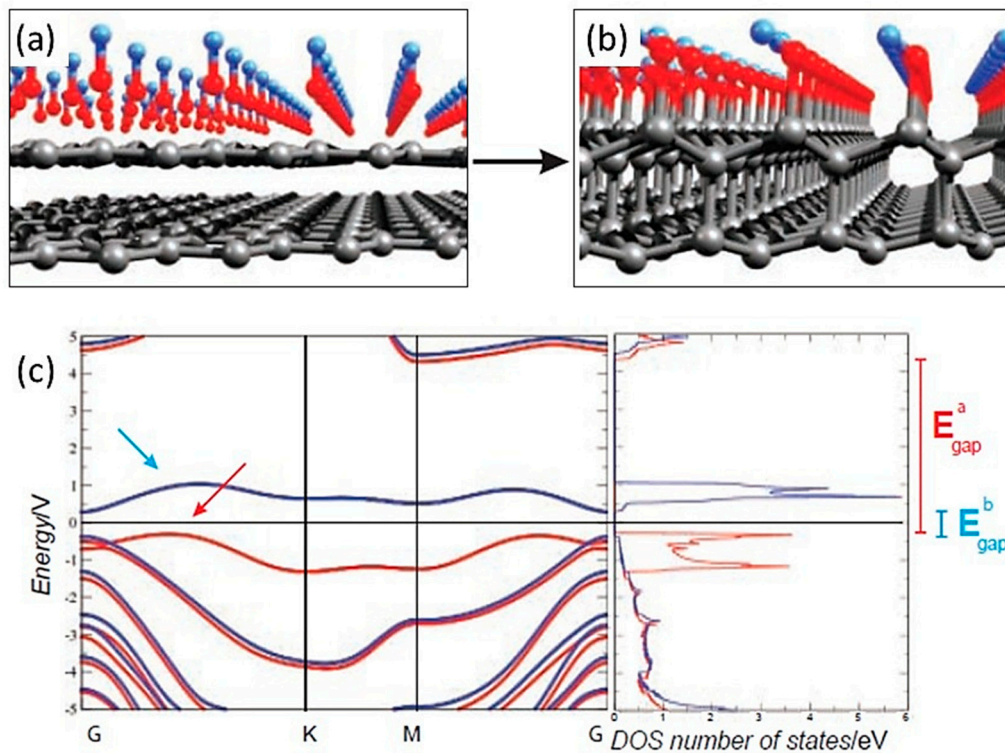

Figure 5. The initial structure with hydroxyl groups on bigraphene (**a**) and diamandol (**b**); the spin-dependent electronic dispersion of the bond spectrum (**c**) and the density of states (DOS) for the unit cell of the Don structure (**c**). The red and blue colors indicate spin-up and spin-down components, respectively [26].

Later, evidence of diamondene formation was provided by Raman spectroscopy studies of two-layer graphene under high pressure [7]. The existence of this 2D rehybridized carbon material has been demonstrated by atomic force microscopy experiments, which have monitored the charge injection into graphene mono- and bilayers with increasing tip-force interaction and different water contents on the graphene surface. Ab initio calculations and molecular dynamics simulations of the transformation of graphene layers under high pressure in the presence of these chemical groups have confirmed previous results [7,26] and have been employed to clarify the mechanism of diamone formation, which requires two or more layers of graphene subjected to high pressures in the presence of specific chemical groups such as hydroxyl groups or hydrogens [30].

1.3. Multilayer Diamanes—Theoretical Studies

Let us dwell on the previous theoretical studies on diamanes formed from two- or three-layered graphenes by full hydrogenation or fluorination. The functionalization effects on the electronic and elastic properties of diamanes formed from two- or three-layered graphenes were considered in [20]. The atomic structure of the diamane could be represented as a stack of covalently bonded monatomic carbon layers (Figure 6a,b). Changing the stacking sequence allows constructing different diamane polytypes. Accordingly, diamanes can be classified as D(ijk … l), where i, j, k and l are position-layer types that can be equal to A, B, or C. For example, two- and three-layered diamanes with a natural diamond stacking sequence (ABCABC …) are denoted as D(AB) and D(ABC); two- and three-layered diamanes with a lonsdaleite stacking sequence (AAA …) are denoted as D(AA) and D(AAA). In the left part of Figure 6a,b, the D(AB) and D(ABC) structures are presented, whereas on the right, the possible stacking sequences for the graphene layers in the corresponding diamanes are shown. As the number of layers increases, because the inner layers cannot be hydrogenated, diamane-related materials can be more accurately described as surface-hydrogenated diamond or lonsdaleite or, more generally, diamanoïds [31]. The graphane structure does not contain any diamond-like cells [4].
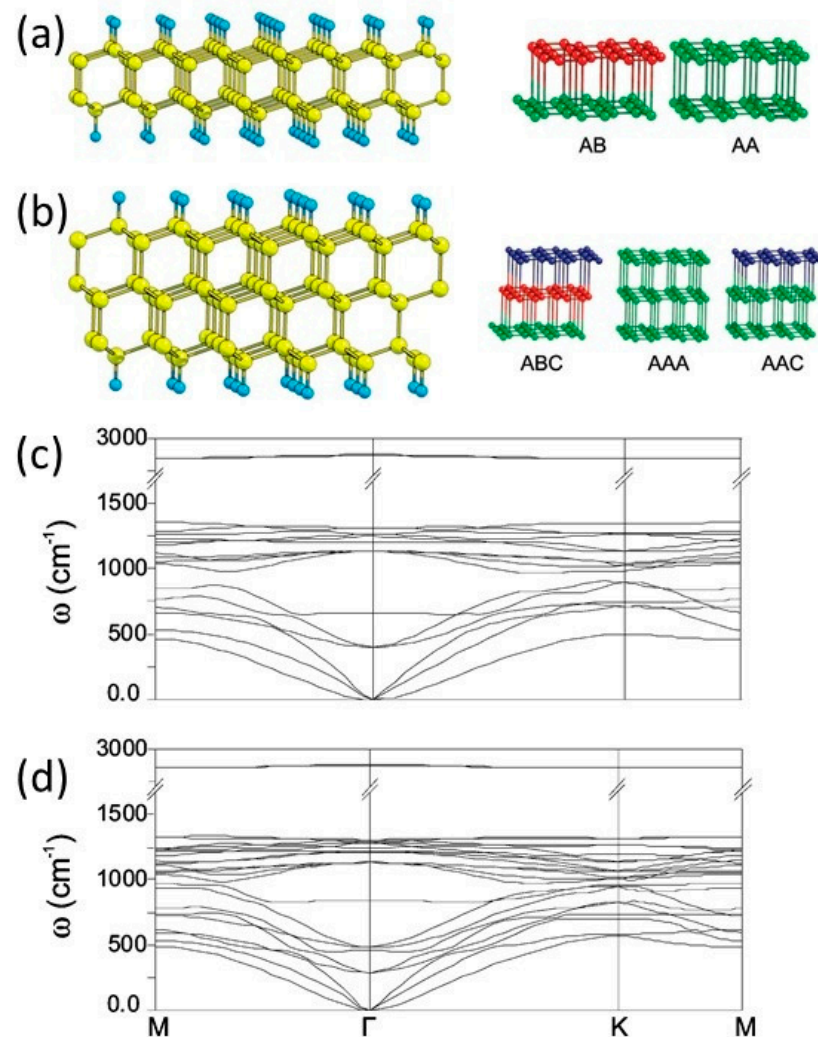
Figure 6. The atomic structure of two-dimensional diamond-like films formed from two and three graphenes: (**a**) diamane D(AB) with AB stacking of two graphene layers; (**b**) diamane D(ABC) with ABC stacking of three layers. Carbon atoms are marked in yellow (light gray); hydrogen is marked in blue (gray). Phononic band structures of each diamane are presented in (**c**) for D(AB) and (**d**) for D(ABC) [20].

The computed formation energies of the structures tend to be almost linearly related to the energy of the bulk diamond and the hydrogen content. The diamanes with diamond-type layer stacking (AB and ABC) display lower energy per atom than corresponding structures with other stacking sequences, but the difference in the energy of the diamanes with diamond and other stacking sequences is smaller than 0.02 eV/atom, which justifies the possible existence of diamanes with any stacking type. Two-layered diamanes D(ij) are less favorable than graphane but more favorable than graphene [20]. The bandgaps of the studied structures should tend to the bandgap of bulk diamond upon a decrease in hydrogen content (and increase in the thickness of the structure). Increasing the number of layers in diamane will lead to the transition of a direct bandgap to an indirect one for diamond.

In order to identify diamanes and be able to estimate their mechanical and thermal properties, it is necessary to study their phononic spectra. The computed phononic band structures of graphane, D(AB) and D(ABC) are presented in Figure 6c,d. The energy splitting of the highest Raman-active modes in the spectra of the diamanes (2865 and 2875 cm^{-1} for D(AB) and 2874 and 2882 cm^{-1} for D(ABC)) was smaller than the energy splitting of the graphane modes (see group VI in Table 2).

Table 2. Phonon frequencies (cm^{-1}) at the Γ-point region and velocities of transverse and longitudinal acoustic in-plane modes (10^3 m/s) [20].

ω_{opt} Groups							
I	II	III	IV	V	VI	V_{TA}	V_{LA}
Graphane	-	-	-	1123, 1123	1159, 1162, 1162, 1328, 1328, 2856, 2896	12.0	17.7
D(AB)	401, 401		664	1131, 1131, 1133, 1133	1201, 1249, 1260, 1260, 1313, 1313, 2865, 2875	12.1	17.8
D(ABC)	291, 291	467, 483, 483	848	1132, 1132, 1133, 1133	1211, 1224, 1224, 1248, 1282, 1287, 1287, 1308, 1308, 2874, 2882	12.2	18.0
Diamond (experiment)						12.4	18.3

The increase in the mode number in the frequency region around 1332 cm^{-1} (diamond fingerprints) could be an indication of diamane films due to a linear increase in the line intensities with the thickness of the diamond-like film (group V in Table 2). Another characteristic feature of diamanes is the appearance of the vibrational modes at 664 and 848 cm^{-1} in the cases of D(AB) and D(ABC), respectively (group III in Table 2). Near the 500 cm^{-1} frequency region, one can see two (for D(AB)) and five (for D(ABC)) optical modes bunched into one and two groups, respectively (groups I and II in Table 2).

Three acoustic branches in diamanes correspond to in-plane (two branches, linear dependence $\omega(k)$) and out-of-plane (one branch, quadratic dependence $\omega(k)$) vibrations of the 2D structure. Increasing the thickness of the film leads to the gradual transformation of the quadratic branch to a linear one with a transverse mode typical for the crystal.

The velocities of the longitudinal and transverse acoustic in-plane modes (Table 2) were obtained from the phononic spectra (Figure 6c,d). For comparison, the longitudinal and transverse velocities were calculated for diamond in a hexagonal orientation based on the experimentally determined elastic constants [32]. The velocities gradually increased with the thickness of the films due to the stiffening of the structures and tended toward the diamond's values. Based on the velocities, the elastic constants of graphene, graphane, D(AB) and D(ABC) were calculated and compared with experimental data for graphite [20].

The mechanical properties of diamane under tension and bending were recently studied using molecular dynamic methods [33]. Similar Young's moduli are found in the zigzag and armchair directions, whereas a much larger fracture strain/strength is observed along the zigzag direction. The layer-stacking sequence exerts a negligible influence on the mechanical properties of diamane. The fracture of diamane is dominated by crack propagation along zigzag directions, independent of the tensile direction. The Young's

modulus and fracture strain/strength decrease when the temperature increases. These results enable a fundamental understanding of the mechanical behavior of diamane, which should benefit its use in nanomechanical devices.

The deformation of diamanes can significantly influence their thermal conductivity [13]; it is predicted that under 5% tensile strain, at room temperature, the thermal conductivity (1081 W/mK) is only about 50% of that of a strain-free sample, and under 20% strain, it is dramatically reduced to only about 11% (226 W/mK). Under applied external strain of 5% leads to the underestimation of the relaxation time with thermal conductivity reduction to 20% compared with strain-free condition. High ballistic thermal conductance (2.95 GW/m2K) has also been demonstrated, and the mean free path is estimated to be 700 nm at room temperature.

The calculation of the energy barriers for the transformation of two- or three-layered graphenes into diamanes was considered by L. Zhu et al. [34]. The hydrogenation of few-layered graphene (FLG) and energy barrier calculations by the climbing image nudge elastic band method incorporated into the VASP [35] were performed, and the results are presented in Figure 7. It was shown that very small energy barriers are needed for forming diamanes based on two and three graphene layers.
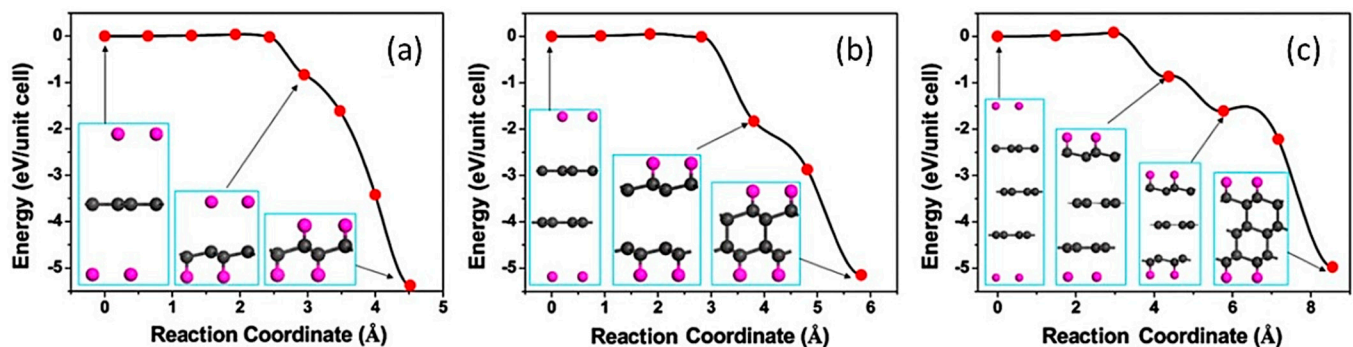

Figure 7. Model of few-layered graphene (FLG) hydrogenation resulting in a thin diamond-like film with the results of energy barrier calculations: (**a**–**c**) are the hydrogenation of single-, double- and triple-layer graphene. The initial configuration is selected so that H atoms (violet balls) are above or below planar FLG [34].

The hydrogenation of FLG films followed by a transformation to diamond films is feasible when FLG is exposed to hydrogen plasma. Though the barrier for FLG hydrogenation is negligible, a significant difference in formation energy exists, which is consistent with some experimental observations that the hydrogenation of single-layer graphene is easier than that of a graphene bilayer. Motivated by the controversial experimental conclusions regarding the affinity of FLG for hydrogen plasma, the hydrogenation of FLGs was systematically investigated within the framework of density functional theory. The very low transition barrier for FLG hydrogenation indicated the feasibility of such hydrogenation through the proposed mechanism. In this work, the electronic properties of the studied diamanes and the hydrogenated graphene bilayer ribbons were also studied.

1.4. Phase (P-T) Diagram of Quasi-Two-Dimensional Carbon Formations

Later, our group developed a mechanism for the phase pressure–temperature (P–T) transitions of many-layer graphenes into multilayered diamanes [35]. First, the Gibbs free energies were computed by the ab initio method to assess the stability of diamond films with pristine surfaces and to determine the critical thickness at which a diamond would split into a stack of graphene layers. A (P, T, h) phase diagram was obtained, showing the conditions for the formation of diamond films from multilayered graphene, where h is the thickness of the film (Figure 8). The authors then evaluated the formation of diamond films facilitated by passivation (of atomic H) on the multilayer graphene surface and found that the pressure of the phase transition was reduced and formally turned

negative, which is practically unnecessary. This phenomenon was named "chemically induced" phase transition, where chemistry and compression concurrently drive diamond film formation. Finally, the atomic structures and phase diagrams for both clean and hydrogenated diamond films with (110) surfaces were studied. The obtained (P, T, h) phase diagram showed the conditions for diamond film formation from multilayered graphene. Figure 8 shows their main results based on calculations [35].
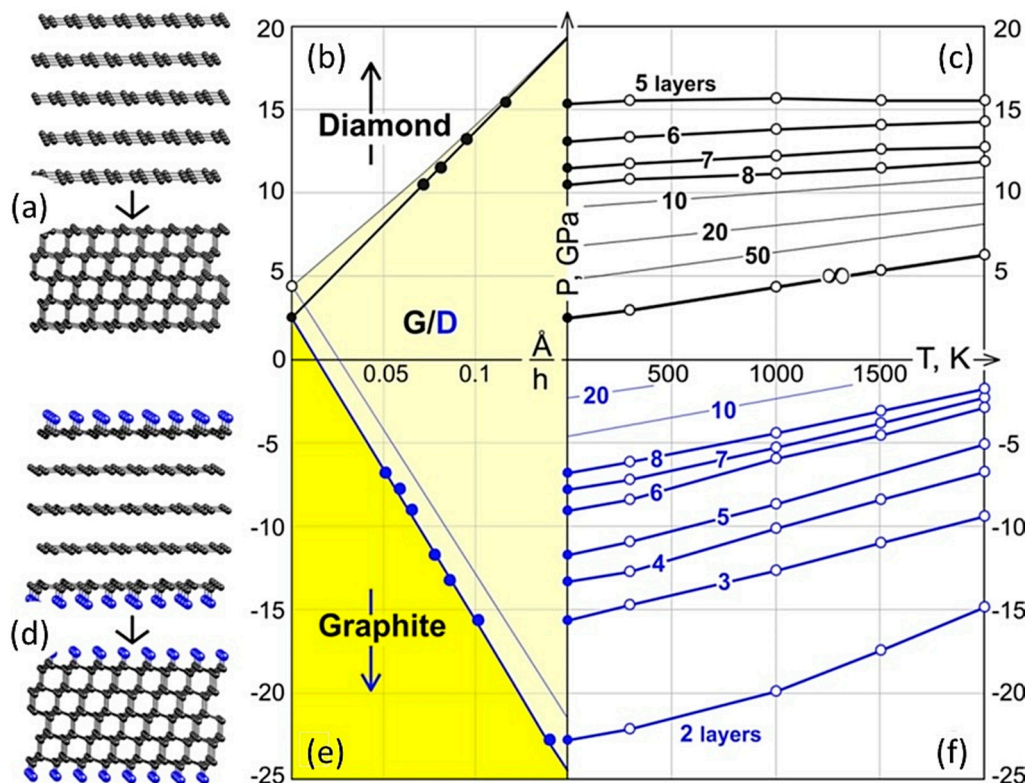

Figure 8. (**a**) Atomic structures of a five-layer graphene and the corresponding diamond film with a pristine surface. (**b**) The dependence of the phase transition pressure P on the inverse film thickness h at T = 0 and 1000 K (solid and thin lines) for films with pristine surfaces. (**c**) The phase diagram (P–T) for the different numbers of n-layer graphenes in diamanes (thin lines show equilibrium curves for *n* = 10, 20 and 50 layers). (**d**) Atomic structure of a five-layer graphene and the corresponding diamond film with hydrogenated surfaces. (**e**) The dependence of the phase transition pressure on the inverse film thickness h at T = 0 and 1000 K (solid and thin lines) for films with hydrogenated surfaces. (**f**) The phase diagram (P–T) for the transition from a multilayer graphene to a diamane film (H is shown in blue; thin lines show the equilibrium curves for *n* = 10 and 20) [35].

The phase transitions were studied for films with both passivated and clean surfaces and for different crystallographic orientations. The phase diagrams for both hydrogenated and clean diamond films with (110) surfaces were carefully mapped out. It was found that chemically induced phase transitions should occur in a similar manner as for the (111) diamond films. The effect of "chemically induced" phase transitions was studied in detail but only from a thermodynamics standpoint.

1.5. Diamanes with Lonsdaleite Structure—Theoretical Studies

Another method of hydrogen adsorption on FLG using a "boat" H-C-C-H configuration for the formation of diamanes with a lonsdaleite structure (hexagonal diamond) was studied in [36]. An investigation of the electronic properties of films with different crystallographic orientations of the surface (Figure 9) found that, in contrast to graphane, diamond films display semiconducting properties with an effective mass close to that of bulk diamond. All the hydrogenated films display direct bandgaps with nonlinear

quantum confinement responses dependent upon the thickness, whereas films with clean surfaces display both metallic and semiconducting electronic structures depending on the surface orientation. The elastic properties of the structures were studied; it was found that such films are stiff but flexible and can be elastically bent out of plane. Comparing the elastic constants and acoustic velocities of lonsdaleite diamanes with those of diamond films of the same thickness shows that, in stiffness, the diamanes are second only to bulk lonsdaleite and graphene (Figure 9g,h).
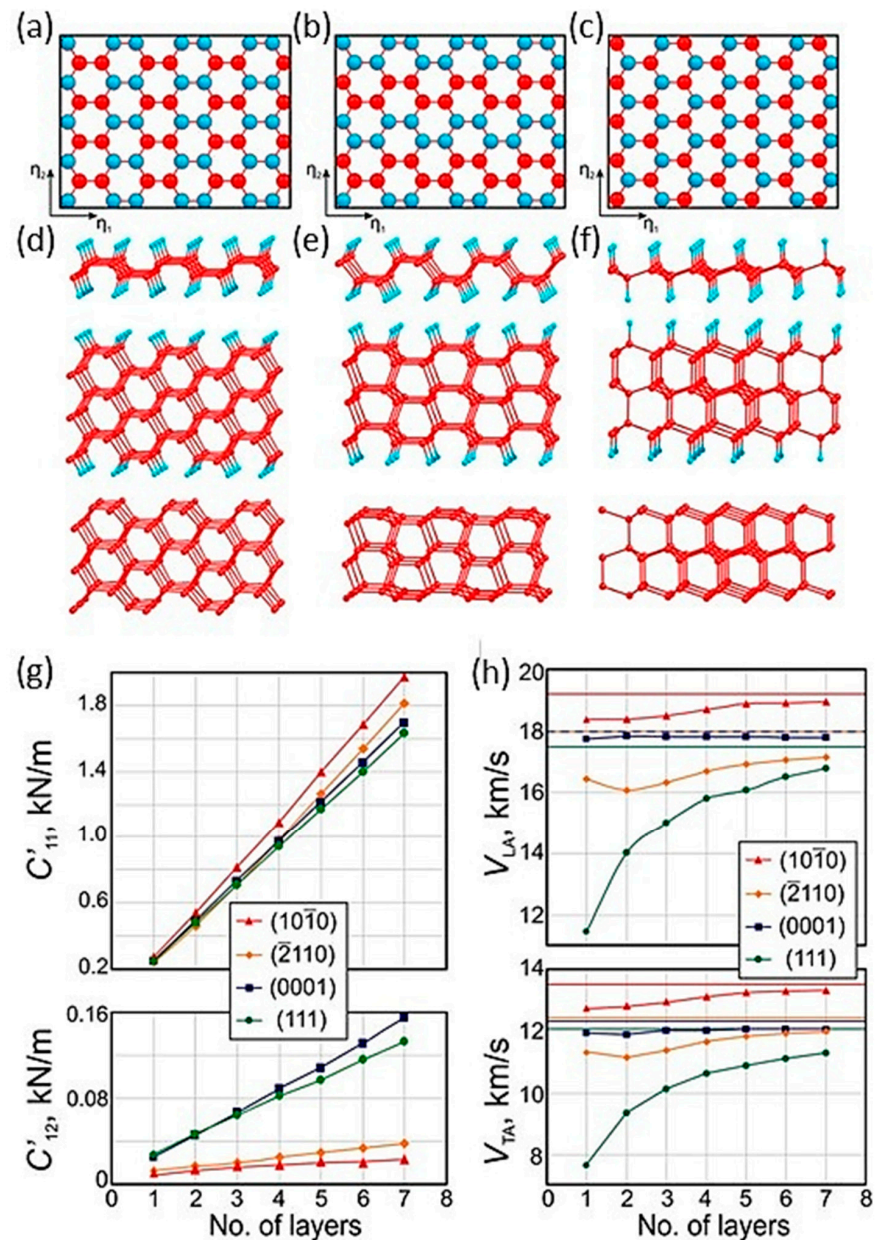

Figure 9. Schemes of the hydrogen coverage of the conformers—non-Bernal-stacked multi-graphene (**a**) "boat1", (**b**) "boat2" and (**c**) "chair1"—showing the atomic structures of the considered graphane conformers and corresponding three-layered lonsdaleite films with hydrogenated and clean surfaces with (**d**) (10$\bar{1}$0), (**e**) ($\bar{2}$110) and (**f**) (0001) crystallographic orientations. Dependence of the (**g**) elastic constants C11′ and C12′ and (**h**) velocities of the longitudinal V_{LA} and transverse V_{TA} acoustic waves of the lonsdaleite films with (10$\bar{1}$0) (▲), ($\bar{2}$110) (◆) and (0001) (■) surfaces for different numbers of layers in comparison with diamond films with (111) surfaces (●) [36].

Thermodynamic theory coupled with atomistic first-principles computations predicts a reduction of not only the required pressure ($p/p_\infty > 1 - h_0/h$, where p_∞ is the pressure flipping the balance to diamond for the infinite phase), but also the nucleation barriers, important for the kinetic feasibility of diamane formation [14]. Moreover, the optimal adsorbent chair pattern on a graphene bilayer results in a cubic diamond lattice, while for thicker precursors, the adsorbent boat structure tends to produce hexagonal diamond (lonsdaleite), if the graphene is AA′ stacked to begin with. As adsorbents, H and F are conducive to diamond formation, while Cl appears to result in steric hinderance.

1.6. Experimental Studies of Diamanes

Prof. F. Piazza's group conducted experiments on "pure" diamanes—2D diamond films completely covered by H atoms [31,37,38]. A low temperature and applied pressure lead to a transformation to ultrathin crystalline carbon films, which were successfully prepared by F. Piazza et al. [37]. They presented a significant technological advance by introducing the hot filament process for the efficient hydrogenation of FLG and the subsequent formation of crystalline and ultrathin sp^3-carbon sheets: a new route for $C(sp^2)$-to-$C(sp^3)$ allotropic transformation. Nanosized and crystalline sp^3-bonded carbon materials were prepared over large surface areas up to ~33 × 51 μm^2 from the exposure of FLG to H radicals produced at low temperature (below 325 °C) and pressure (50 Torr). Sp^3-C-related peaks from diamond and/or lonsdaleite and/or hybrids of both were detected in UV and visible Raman spectra (Figure 10a,b), peaks that were close to the peaks of earlier Raman spectra computed for diamanes [39].
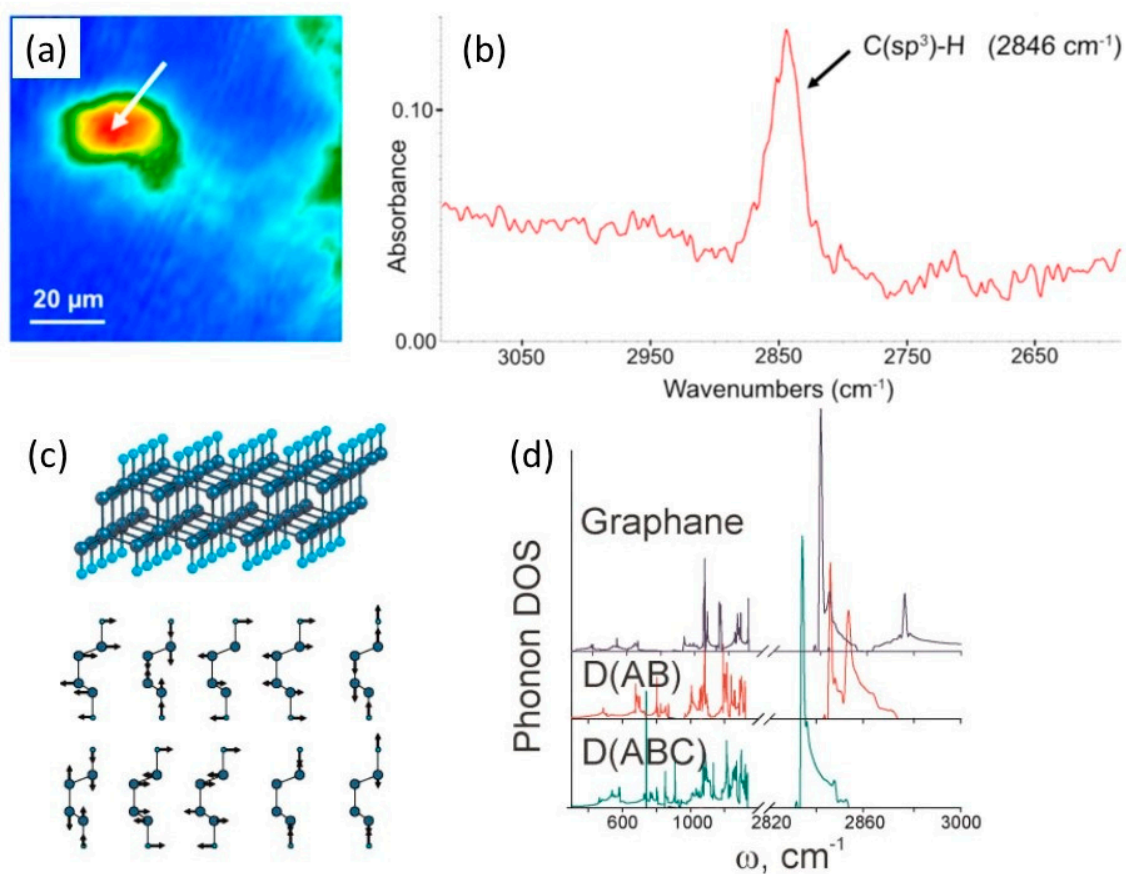
Figure 10. (**a**) FTIR mapping of a large-sized circular area of ~150 mm^2 containing C-H bonds (marked by the arrow) and (**b**) absorbance spectra taken in the region identified by an arrow [37]. (**c**) Calculated atomic structure and vibration pattern of optical modes of diamane and (**d**) phonon densities of the states of graphane and diamanes [39].

Piazza's group [31] next confirmed the successful conversion of few-layer graphene into nanometer-thick and crystalline sp^3-C sheets. The number of graphene layers in the starting FLG was higher than 2–3, and the sp^2-C to sp^3-C conversion was only partial. Partial conversion generates couples of twisted, superimposed coherent domains (TCDs), supposedly because of stress relaxation, which is evidenced by electron diffraction and Raman spectroscopy data. TCDs occur along with a twisted bilayer graphene feature located at the interface between the upper diamanoïd domain and the non-converted graphenic domain underneath. The phonon dispersion of the ABBA-stacking model (Figure 11a–c) was investigated, and upon full atomic relaxation, all the frequencies remain positive (Figure 11d), proving the stability of the structure. The T bands of the phonon dispersion corresponded to the interface between the sp^2-C layer and hydrogenated sp^3-C layer (Figure 11e).
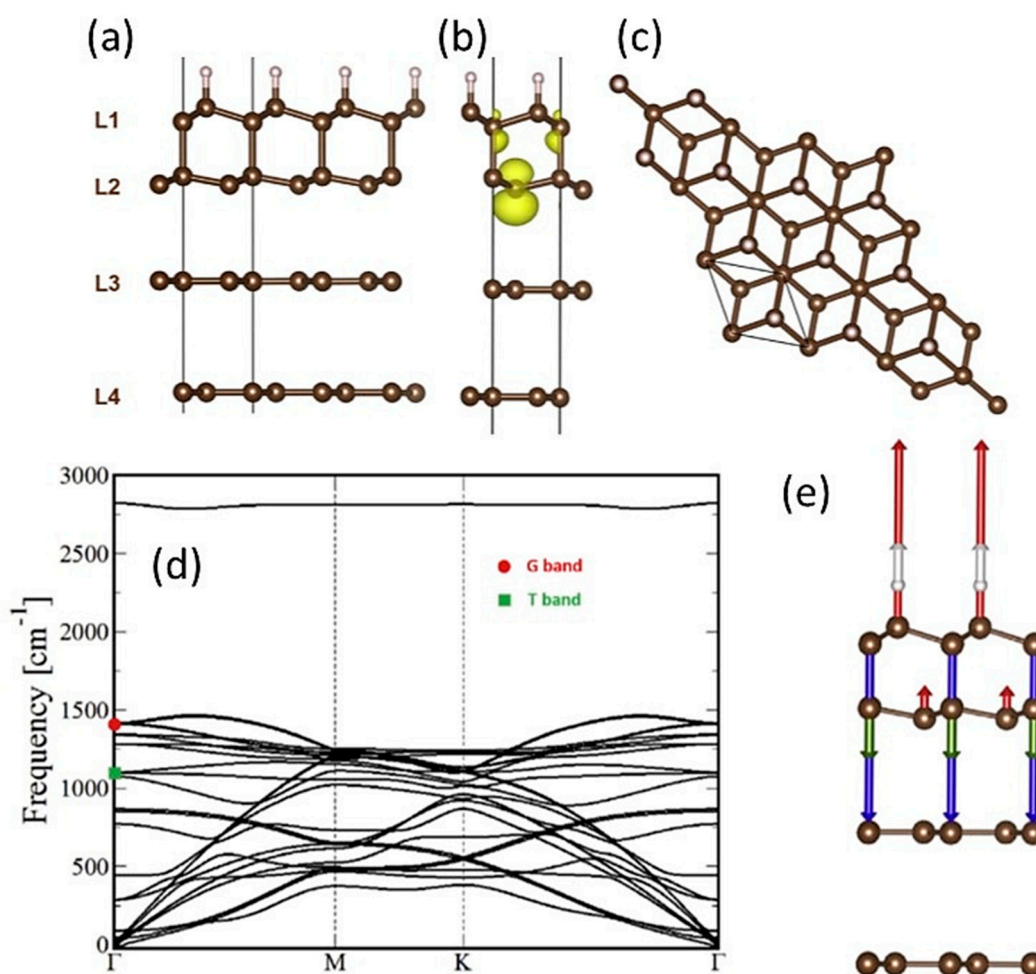
Figure 11. Computed model: (**a**,**b**) are two side views, and (**c**) is a top view of the upper-layer-hydrogenated FLG used in density functional theory (DFT) calculations with ABBA-stacking graphene [31]. In (**b**) is shown how the pz orbitals are preferably oriented towards the layer underneath (layer L3). The projected structure (**c**) is that of the face-centered cubic of diamond with the unit cell (black lines). (**d**) Phonon dispersion curves of the model in (**a**). (**e**) Corresponding vectors of the atomic vibrations along the normal T mode at 1078 cm^{-1}.

Reference [38] reported the first evidence for the successful synthesis of genuine diamane. Micro-Raman mapping was performed before (Figure 12a) and after (Figure 12b) exposure to the hydrogenation process promoted by hot filaments. Before hydrogenation, the spectra of the graphene bilayer were characterized by a regular sharp G peak at around 1582 cm^{-1}, which is due to the bond stretching of all the pairs of sp^2-C in the graphene sheets. After hydrogenation, drastic changes can be observed in the Raman spectra. The

typical spectrum of such a region exhibits specific features: (i) the G peak is no longer detected; (ii) the D peak that originates from defects in the graphene sheets is not observed either; (iii) a sharp peak at around 1344–1367 cm^{-1} occurs.
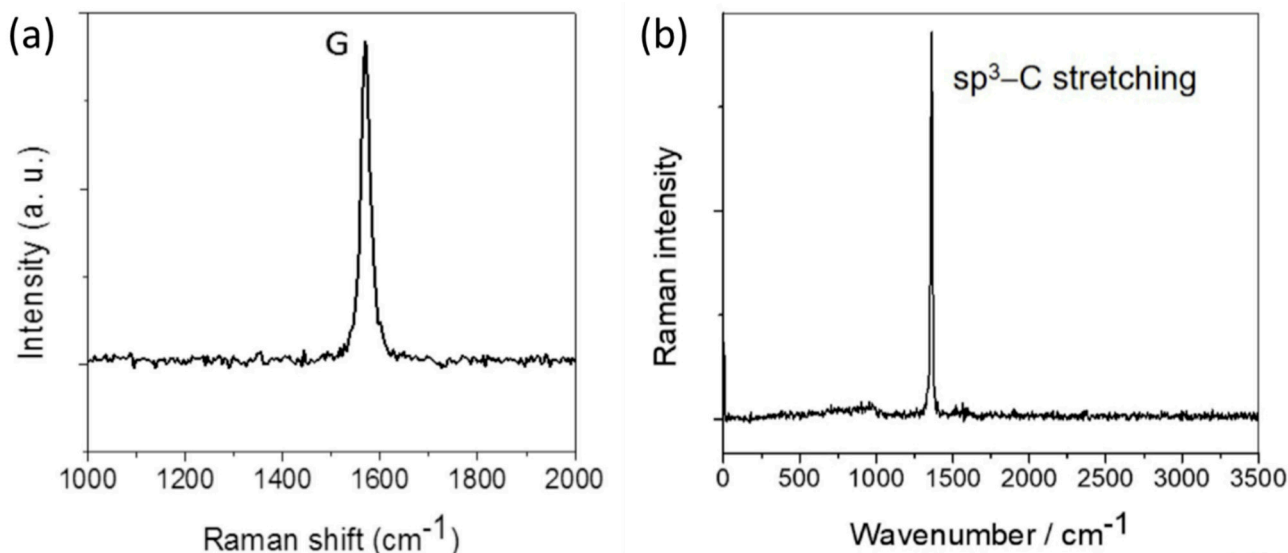
Figure 12. UV Raman spectra (at 244 nm) of few-layer graphene before (**a**) [37] and after hydrogenation (**b**) [38].

The experimental results [31,37,38] were compared to computational predictions, suggesting that the sp3-C materials obtained are ultrathin films with hydrogenated basal planes. The preparation method used by Piazza's group [38] opens the door to the large-scale production of 2D diamond-like films.

1.7. Fluorinated Diamanes—Theoretical and Experimental Studies

It is well established that fluorine is more effective for forming covalent bonds with carbon than hydrogen. The first study of fluorinated graphene was an ab initio investigation by J. Sivek et al. [5] into the stability and electronic properties of a fluorinated graphene bilayer, F-diamane, comparing its properties with those of graphene and diamanes—hydrogenated one- and two-layer graphenes [2,3,22]. It was found that the calculated bandgap for F-diamane exceeded that for diamanes by 30%, and it was almost as strong as graphene.

Later, the elastic and electronic properties of quasi-two-dimensional cubic and hexagonal (lonsdaleite structure) F-diamane films based on multilayered graphenes (Figure 13a) were studied using ab initio calculations. It was found that both types of films display stiffnesses comparable with those of bulk diamond. The hexagonal diamond films display the most remarkable properties, combining the highest longitudinal stiffnesses with the smallest Poisson's ratios. DFT-PBE and GW approaches predicted essential differences in electronic properties. PBE functionally predicts the nonmonotonic dependencies upon the film thickness of the bandgap value (Figure 13b), effective electron and hole masses, and bandgap's rate of response to changes in mechanical strain.

A high mechanical stiffness could be useful for the application of F-diamane films as nanoscale elements in nanoelectronics. The wide bandgap suggests the application of the films as ultrathin insulating nanolayers, whereas the presence of a direct type of energy gap in the thinnest films could be useful in nanophotonics.

Most recently, a fluorinated diamond monolayer called "F-diamane" has been successfully experimentally realized via the fluorination of a graphene bilayer by P.V. Bakharev et al. [40]. They created stable F-diamine (based on an AB-stacked graphene bilayer) over a large area by chemical vapor deposition on a single crystal CuNi(111) surface at 1 atmosphere of pressure. Regrading hydrogenated graphene, it is impossible to quantitatively distinguish between C(sp^3)–H and C(sp^3)–C(sp^3) bonds in the C1s XPS spectrum [7]. In

contrast to hydrogen, fluorine can be "directly" identified by XPS (X-ray photoelectron spectroscopy), EDX (energy dispersive X-ray) and EELS (electron energy loss spectroscopy).
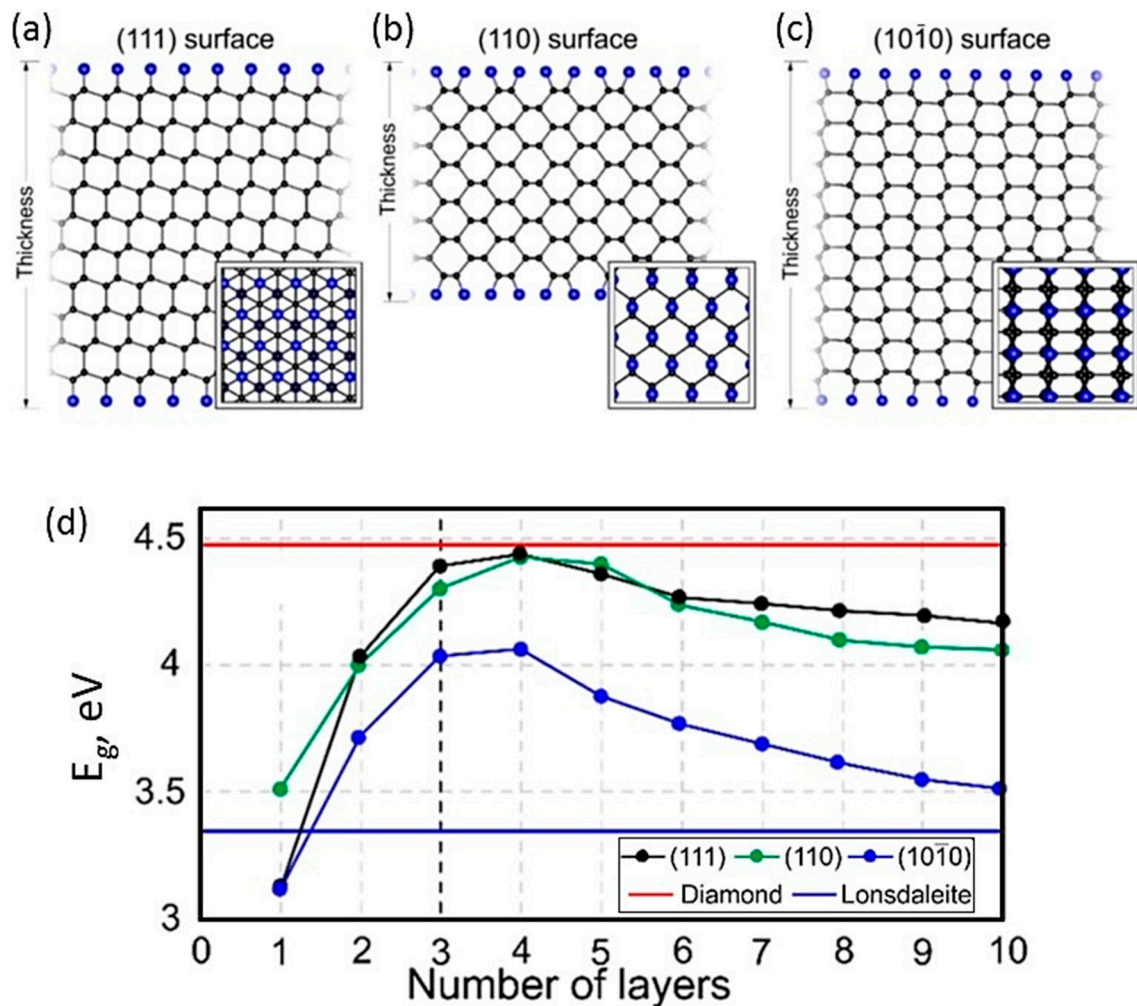
Figure 13. Atomic structures of considered fluorinated films [6] with 10 layers with (**a**) (111), (**b**) (110) and (**c**) (10$\bar{1}$0) surfaces (top views of the films shown in the insets; black color is carbon, and blue is fluorine), and (**d**) dependence of the bandgaps of the fluorinated cubic diamond films with (111) and (110) surfaces and hexagonal diamond film with (10$\bar{1}$0) orientation upon the number of layers (red horizontal lines are the bandgap of single-crystal diamond; blue lines correspond to bandgap of bulk lonsdaleite) [6].

First, according to the Pauling scale, the electronegativities of carbon, hydrogen and fluorine are 2.55, 2.20 and 3.98, respectively. Covalent C–F bonds are strongly polarized toward the F atom. Therefore, a fluorinated graphene structure can be quantitatively characterized using XPS due to a strong binding energy shift of the C–F peak towards higher binding energies relative to the C–C (sp^2/sp^3) peaks in the C1s spectrum. This allowed obtaining the configuration and C/F stoichiometry of the fluorinated structure by the X-ray photospectroscopic method. Second, fluorination can be performed under moderate conditions (near-room temperatures and at low/atmospheric pressure), such as by using xenon difluoride (XeF$_2$) vapor as a source of fluorine. The common techniques for graphene require plasma treatment [4], high pressure [7] or methods able to control the H/OH coverage and stoichiometry as well as the degree of the induced defects.

The high-resolution transmission electron microscopy (TEM) results are presented in Figure 14.
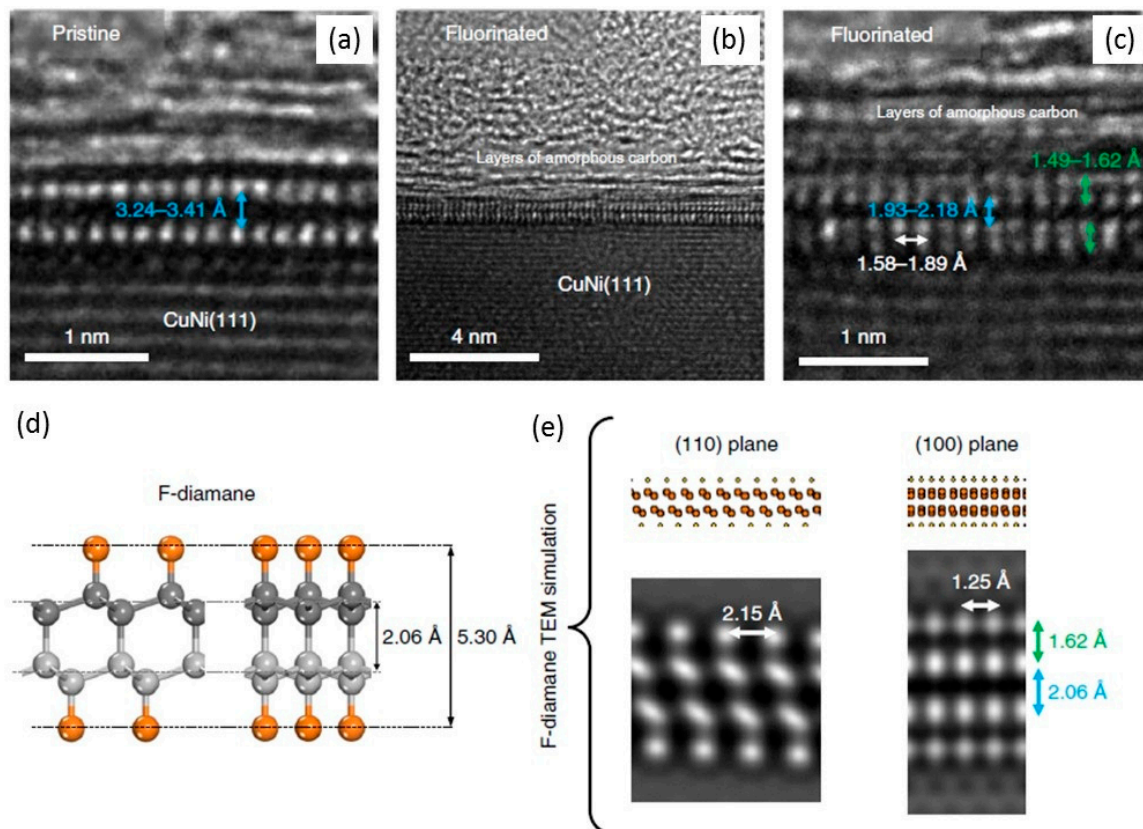
Figure 14. TEM study of F-diamane on CuNi (111) surface. High-resolution cross-sectional transmission electron micrographs of as-grown pristine graphene bilayer (**a**) and Sample A (**b**,**c**); simulated HR-TEM images of DFT-optimized F-diamane (**d**,**e**) [40].

A new fabrication method for few-layered F-diamane sheets was proposed and implemented by X. Chen et al. [41], who synthesized well-dispersed ultrathin $(C_2F)_n$ sheets by the fluorination of graphite and liquid-phase exfoliation in a variety of solvents with a high yield. Another interesting method of F-diamane preparation was proposed in [42], tailoring the full fluorination of bigraphene on rough silicon dioxide (SiO_2) via substrate interactions; the top and bottom bG surfaces are fluorinated, while only the top surface of the bigraphene on the flat hBN substrate is fluorinated.

The fluorinated diamane is an ultrathin material with a direct, wide bandgap larger than that of hydrogenated diamane. Its elastic modulus is comparable to that of graphene and higher than those of most other 2D materials. The authors [43] show that the tensile strength is dictated by the soft-mode phonon instability under uniaxial tension and the elastic instability under biaxial strain. They also found that the calculated electron mobility (2732 $cm^2V^{-1}s^{-1}$) and hole mobility (1565 $cm^2V^{-1}s^{-1}$) in these two diamond-like monolayers were superior to those of III-V semiconductor compounds.

The studied and obtained semiconducting F-diamane films with wide bandgaps have potential for applications in nanoelectronics, nano-optics and nano-electromechanical systems.

1.8. Moiré Diamanes—Theoretical Studies

Recently [44], new types of diamanes based on Moiré commensurate bilayered graphene [45] with twisted angles close to 30° were studied ab initio. They were chosen based on the special atomic structure of these bigraphenes—the presence of C-C and C′-C′ bond crossings (Figure 15a,b), where C and C′ are carbon atoms of the top and bottom layers, respectively. The atoms of these bonds do not combine in the process of diamane formation. They are preferable for the adsorption of atoms or molecules in contrast to ordinary diamanes, where the adsorbed atoms alternate (Figure 15d,e).

The greater vibration freedom of these C-C pairs along the bigraphene normal facilitates the simultaneous adsorption of H-atom pairs to them and the formation of complexes (H-C-C-H/H′-C′-C′-H′), in contrast to the alternating complexes (H-C)/(C′-H′) in ordinary diamanes. Such H-C-C-H complexes are well-established in "boat"-type graphene [46] and lonsdaleite-like diamanes [23,36]. The paper [47] notes that H-C-C-H complexes can be advantageously formed on the graphene surface under special conditions.
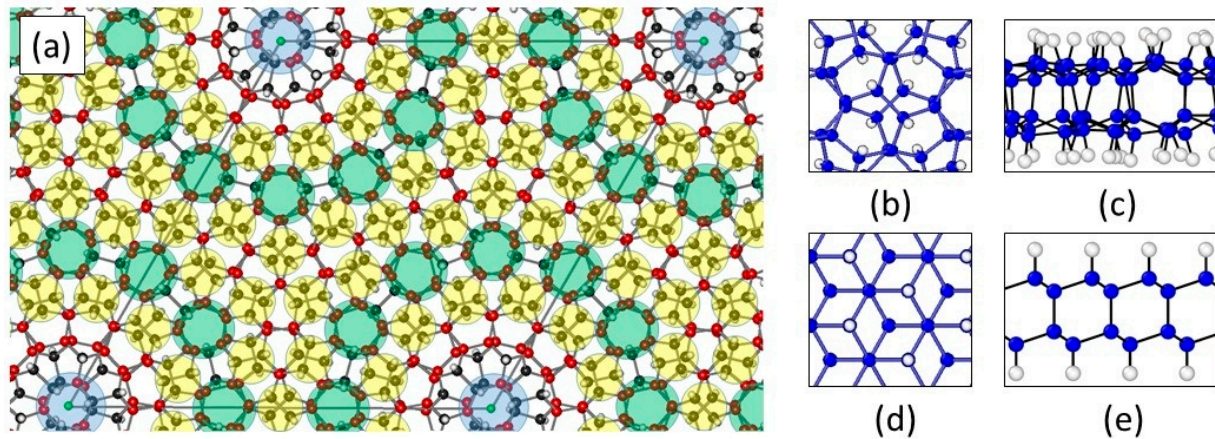
Figure 15. Top (**a,b**) and side (**c**) views of the Dn29.4 atomic structure with H-C-C-H and H′-C′-C′-H′ crossing complexes in yellow rings and 5-5′ and 3-3′ C-C′ bonds in green and blue rings, respectively; top (**d**) and side (**e**) views of the structure of ordinary AB diamane. Dark atoms in (**a**) adsorb light atoms of hydrogen (or fluorine). The C-C′ length distribution in Dn29.4 is related to the deviation of some interlayer bonds from the normal direction of the 2D film (**b,c**) in contrast to all the C-C′ bonds in ordinary diamane (**d,e**). Rhombus is unit cell of these Moiré diamanes [44].

A fully sp^3-hybridized diamane structure can be formed after H or F adsorption on both sides the bigraphene with twisted angles close to $30°$. First, fully sp^3-hybridized diamane structures formed after H or F adsorption on both sides of the bigraphene with twisted angles of $29.4°$ were studied. The remaining carbons were transformed into sp^3 C atoms connected by the interlayer C-C′ bonds. This Moiré diamane is shown in Figure 15a–c. For comparison, we show a fragment of the ordinary diamane structure based on AB-stacking BG (Figure 15d,e). The results of the ab initio computations are dielectric gaps of 3.6 and 4.1 eV for Dn29.4 and F-Dn29.4, respectively.

Then, the Moiré diamanes Dn27.8, F-Dn27.8, Dn21.8 and F-Dn21.8, based on commensurate bigraphenes with twisted angles of $27.8°$ and $21.8°$, were studied. The results of the atomic and electronic structure calculations performed using the VASP package are shown in Table 3.

Table 3. Formation energies E_f of sp^3 $C_M X_N$ (X = H, F) structures relative to graphene, and bandgaps E_g of the considered Moiré diamanes [44].

| System	Unit Cell	E_f, eV/Atoms	E_g, eV
Graphane	C_2H_2	−0.11	3.4
F-graphane	C_2F_2	−0.91	3.3
DnAB	C_4H_2	−0.03	3.1
F-DnAB	C_4F_2	−0.5	4.0
Dn21.8	$C_{28}H_{18}$	0.12	3.2
F-Dn21.8	$C_{28}F_{18}$	−0.19	4.2
Dn27.8	$C_{52}H_{30}$	0.13	3.3
F-Dn27.8	$C_{52}F_{30}$	−0.29	4.5
Dn29.4	$C_{388}H_{174}$	0.14	3.6
F-Dn29.4	$C_{388}F_{174}$	−0.28	4.1
Diamond	C_8	0.12	4.2

The electronic densities of the states of the Moiré diamanes are shown in Figure 16a,b. The insets in Figure 16 show top views of the atomic structures of these 2D diamond-like films. It can be observed that the F-Dn27.8 structure has the largest ultra-wide dielectric gap, 4.5 eV, even slightly exceeding the bandgap of diamond, 4.2 eV.
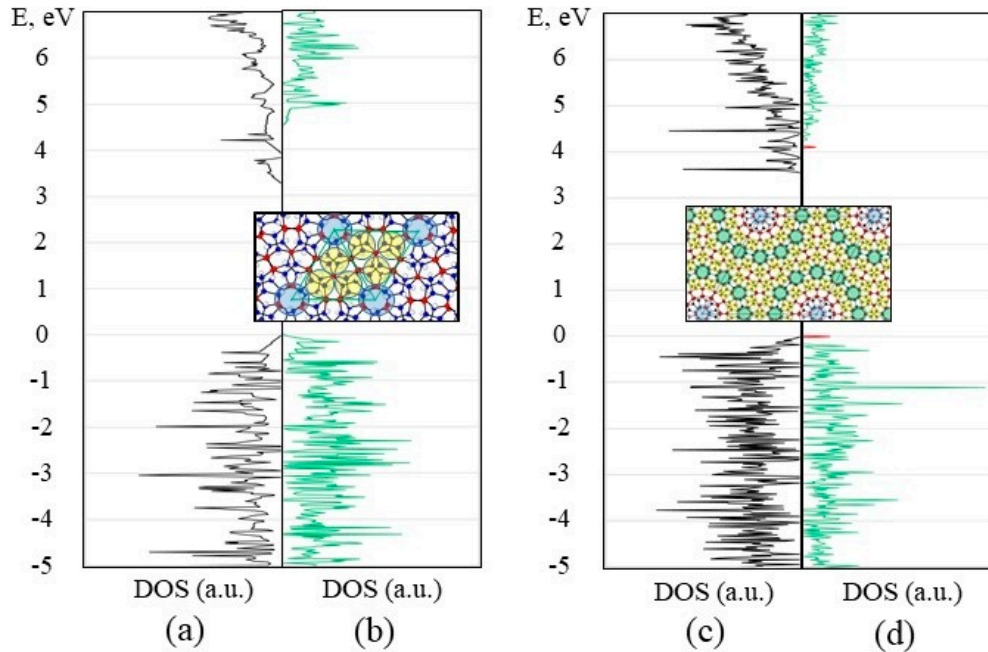
Figure 16. Density of electronic energy states (DOS) for Dn27.8 (**a**) and F-Dn27.8 (**b**) diamanes, with bandgaps of 3.3 and 4.5 eV, and Dn29.4 (**c**) and F-Dn29.4 (**d**) diamanes, with bandgaps of 3.6 and 4.1 eV, respectively. Insets—relevant structures with unit cell rhombuses [44].

As shown above, when identifying structures, experiments based on the Raman and IR scattering of light are of great importance—from their spectra, one can unambiguously determine the atomic structure of the material under study, making the calculation of these spectra important. However, the difficulty in calculating them for Moiré structures is associated with the large number of atoms in the unit cells of such crystal structures.

The third commensurate structure, with a twisted angle of 21.8° [45], has fewer C atoms in its unit cell than the considered tBGs. Therefore, the Raman and IR spectra of Dn21.8 could also be calculated [48]. Figure 17 shows the Raman spectra of the diamanes Dn21.8 and F- Dn21.8, as examples, which are compared with the spectra of standard diamanes. The results of the computation of the main Raman modes of the diamanes Dn21.8 and F-Dn21.8 are presented in Table 4.
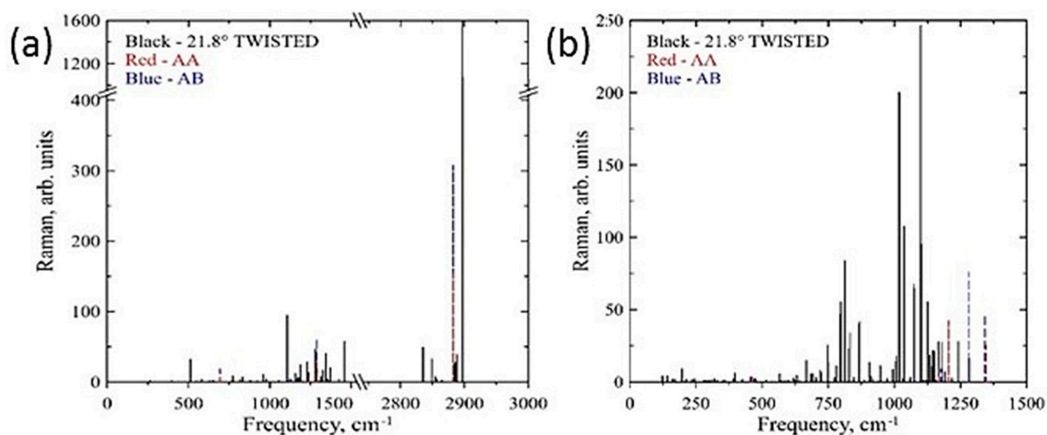
Figure 17. Raman spectra of twisted diamanes Dn21.8 (**a**) and F- Dn21.8 (**b**) in comparison with standard, similar AA- and AB-stacked diamanes [48].

Table 4. Main Raman modes of hydrogenated and fluorinated AB and Dn21.8 diamanes.

System	Frequinces, cm^{-1}				
Dn21.8	1343.9	1344.1	1459.9	2834.9	
F-Dn21.8	797.8	1019.1	1035.5	1073.9	1101.9
DnAB	1272.0	1341.3	2859.4	2868.6	
F-DnAB	1212.0	1282.2	1342.1	1352.4	

We can observe high- and low-frequency Raman shifts (for Dn21.8 and F-Dn21.8) with the presence of active phonon modes polarized parallel to the film surface [48]. This allows the identification of such material in a more simplified measurement through a Raman spectrum scheme.

Moiré diamane systems are different from ordinary diamanes according to two main features, namely, their wide-gap electronic spectra, and the peculiarities of their Raman and IR spectra. The calculated bandgaps of these diamanes—Dn29.4, F-Dn27.8, Dn27.8 and Dn21.8—are substantially wider than the ~3 eV gaps of ordinary diamanes based on non-twisted bigraphenes. The broad DOS peak distribution in the valence and conductive bands suggests promise for these new diamond-like films in ultra-wide-bandgap optoelectronic nanodevices. We found wide-gap electronic spectra, frequency shifts and the presence of optical active phononic modes polarized parallel to the film surface to be characteristic of twisted systems.

A controllable and reproducible way of preparing Moiré diamanes based on the hydrogenation or fluorination of twisted bigraphenes, now successfully performed [49], should be similar to the preparation of ordinary diamanes. These 2D Moiré diamond-like films prepared through fluorination and hydrogenation will enable the creation of new optic and electronic elements made from these new 2D wide-bandgap materials.

Structures based on the twisted bigraphenes partially covered with H (or F) atoms are also interesting. They were theoretically studied in [50–53]. Bigraphenes with twisted angles $\Theta < 15°$ have periodically arranged specific areas that are close to those of AA- and AB-stacking bilayers. The adsorption of H (or F) on these areas leads to the formation of domains of AA and AB diamanes in the twisted bigraphene mesh [50,52,53]. In bigraphenes with angles $\Theta = 30°$ and $\Theta = 27.8°$, hydrogens adsorbed in the circle chain shape lead to the formation of fullerene-like domains in the bigraphene mesh [51]. All these structures can be used as 2D semiconductor films with hybrid structures of sp2 meshes and sp3 domains with different semiconductor bandgaps, with maximum values of about 1–3 eV. Similar structures also have enhanced mechanical properties resulting from the deterministic control of the interlayer twist angles and chemical functionalization [54,55].

High-pressure experiments with bi- and multilayered graphanes show the formation of 2D diamond structures [56,57]. These kinds of diamanes without adsorbents on the surfaces, named diamondenes [56], could serve as diamond seeds in nanoheterostructures and rocks subjected to high pressures.

Recent experiments show evidence for the formation of a hard and transparent sp^3-containing 2D phase during the compression of few-layer graphene samples on a SiO$_2$/Si substrate in water [15]. The Raman spectroscopy data indicate phase transitions and surprisingly similar critical pressures for two- and five-layer graphene and graphite in the 4–6 GPa range. Water has been shown to play a major role in facilitating the phase transition. The authors state that their investigations indicate a novel, surface-to-bulk phase transition mechanism that hints at diamondene formation. In [58], the authors propose and theoretically show the shear-induced diamondization of multilayer graphene at pressures much lower than the high pressure used for the transformation of graphite into diamond. Preparation schemes for diamane-like structures are still under development.

2. Summary

Regarding the ongoing rapid development of a new class of 2D materials, diamanes, all the presented results indicate that they show promise for a wide range of applications.

Despite the many theoretical predictions of the diamane-like structures and their properties, relevant experimental studies are still few. We hope for future progress in experiments related to the synthesis of diamanes and the production of device prototypes.

The diamane type of materials, as stated in the article [37], "opens the door to new research in multiple areas for the development of new potential applications and may have wide scientific impact, including for the understanding of extraterrestrial diamond-related structures".

Institutional Review Board Statement: Not applicable.

Informed Consent Statement: Not applicable.

Data Availability Statement: The data that support the findings of this study are available from the corresponding author upon reasonable request.

Conflicts of Interest: The authors declare no conflict of interest.

References

1. Novoselov, K.S. Electric Field Effect in Atomically Thin Carbon Films. *Science* **2004**, *306*, 666–669. [CrossRef] [PubMed]
2. Novoselov, K.S.; Andreeva, D.V.; Ren, W.; Shan, G. Graphene and Other Two-Dimensional Materials. *Front. Phys.* **2019**, *14*, 13301. [CrossRef]
3. Chernozatonskii, L.A.; Sorokin, P.B.; Kvashnin, A.G.; Kvashnin, D.G. Diamond-like C2H Nanolayer, Diamane: Simulation of the Structure and Properties. *JETP Lett.* **2009**, *90*, 134–138. [CrossRef]
4. Elias, D.C.; Nair, R.R.; Mohiuddin, T.M.G.; Morozov, S.V.; Blake, P.; Halsall, M.P.; Ferrari, A.C.; Boukhvalov, D.W.; Katsnelson, M.I.; Geim, A.K.; et al. Control of Graphene's Properties by Reversible Hydrogenation: Evidence for Graphane. *Science* **2009**, *323*, 610–613. [CrossRef] [PubMed]
5. Sivek, J.; Leenaerts, O.; Partoens, B.; Peeters, F.M. First-Principles Investigation of Bilayer Fluorographene. *J. Phys. Chem. C* **2012**, *116*, 19240–19245. [CrossRef]
6. Kvashnin, A.G.; Avramov, P.V.; Kvashnin, D.G.; Chernozatonskii, L.A.; Sorokin, P.B. Features of Electronic, Mechanical, and Electromechanical Properties of Fluorinated Diamond Films of Nanometer Thickness. *J. Phys. Chem. C* **2017**, *121*, 28484–28489. [CrossRef]
7. Martins, L.G.P.; Matos, M.J.S.; Paschoal, A.R.; Freire, P.T.C.; Andrade, N.F.; Aguiar, A.L.; Kong, J.; Neves, B.R.A.; de Oliveira, A.B.; Mazzoni, M.S.C.; et al. Raman Evidence for Pressure-Induced Formation of Diamondene. *Nat. Commun.* **2017**, *8*, 96. [CrossRef]
8. Zhu, L.; Zhang, T. Suppressed Thermal Conductivity in Fluorinated Diamane: Optical Phonon Dominant Thermal Transport. *Appl. Phys. Lett.* **2019**, *115*, 151904. [CrossRef]
9. Zhu, L.; Li, W.; Ding, F. Giant Thermal Conductivity in Diamane and the Influence of Horizontal Reflection Symmetry on Phonon Scattering. *Nanoscale* **2019**, *11*, 4248–4257. [CrossRef]
10. Zhang, T.; Zhu, L. Sensitively Tuning the Thermal Conductivity of Diamane via Engineering the Mass of Functional Groups. *Nanotechnology* **2020**, *31*, 435409. [CrossRef]
11. Raeisi, M.; Mortazavi, B.; Podryabinkin, E.V.; Shojaei, F.; Zhuang, X.; Shapeev, A.V. High Thermal Conductivity in Semiconducting Janus and Non-Janus Diamanes. *Carbon* **2020**, *167*, 51–61. [CrossRef]
12. Zheng, Z.; Zhan, H.; Nie, Y.; Xu, X.; Qi, D.; Gu, Y. Single Layer Diamond—A New Ultrathin 2D Carbon Nanostructure for Mechanical Resonator. *Carbon* **2020**, *161*, 809–815. [CrossRef]
13. Hu, Y.; Li, D.; Yin, Y.; Li, S.; Ding, G.; Zhou, H.; Zhang, G. The Important Role of Strain on Phonon Hydrodynamics in Diamond-like Bi-Layer Graphene. *Nanotechnology* **2020**, *31*, 335711. [CrossRef] [PubMed]
14. Erohin, S.V.; Ruan, Q.; Sorokin, P.B.; Yakobson, B.I. Nano-Thermodynamics of Chemically Induced Graphene–Diamond Transformation. *Small* **2020**, *16*, 2004782. [CrossRef]
15. Pimenta Martins, L.G.; Silva, D.L.; Smith, J.S.; Lu, A.-Y.; Su, C.; Hempel, M.; Occhialini, C.; Ji, X.; Pablo, R.; Alencar, R.S.; et al. Hard, Transparent, Sp3-Containing 2D Phase Formed from Few-Layer Graphene under Compression. *Carbon* **2021**, *173*, 744–757. [CrossRef]
16. Gupta, S.; Yang, J.-H.; Yakobson, B.I. Two-Level Quantum Systems in Two-Dimensional Materials for Single Photon Emission. *Nano Lett.* **2019**, *19*, 408–414. [CrossRef]
17. Qiu, D.; Wang, Q.; Cheng, S.; Gao, N.; Li, H. Electronic Structures of Two-Dimensional Hydrogenated Bilayer Diamond Films with Si Dopant and Si-V Center. *Results Phys.* **2019**, *13*, 102240. [CrossRef]
18. Li, J.; Yin, H.; Gao, N.; Zhang, M.; Mu, J.; Gao, L.; Li, H. First-Principles Calculations for Li, P Dopants and Vacancy Defect in Ultra-Thin Hydrogenated Diamond Nanofilms: Structural, Electronic and Optical Properties. *Diam. Relat. Mater.* **2019**, *99*, 107526. [CrossRef]
19. Kresse, G.; Furthmüller, J. Efficiency of Ab-Initio Total Energy Calculations for Metals and Semiconductors Using a Plane-Wave Basis Set. *Comput. Mater. Sci.* **1996**, *6*, 15–50. [CrossRef]
20. Chernozatonskii, L.A.; Sorokin, P.B.; Kuzubov, A.A.; Sorokin, B.P.; Kvashnin, A.G.; Kvashnin, D.G.; Avramov, P.V.; Yakobson, B.I. Influence of Size Effect on the Electronic and Elastic Properties of Diamond Films with Nanometer Thickness. *J. Phys. Chem. C* **2011**, *115*, 132–136. [CrossRef]

21. Mortazavi, B.; Shojaei, F.; Javvaji, B.; Azizi, M.; Zhan, H.; Rabczuk, T.; Zhuang, X. First-Principles Investigation of Mechanical, Electronic and Optical Properties of H-, F- and Cl-Diamane. *Appl. Surf. Sci.* **2020**, *528*, 147035. [CrossRef]

22. Leenaerts, O.; Partoens, B.; Peeters, F.M. Hydrogenation of Bilayer Graphene and the Formation of Bilayer Graphane from First Principles. *Phys. Rev. B* **2009**, *80*. [CrossRef]

23. Samarakoon, D.K.; Wang, X.-Q. Tunable Band Gap in Hydrogenated Bilayer Graphene. *ACS Nano* **2010**, *4*, 4126–4130. [CrossRef] [PubMed]

24. Zhou, J.; Wang, Q.; Sun, Q.; Chen, X.S.; Kawazoe, Y.; Jena, P. Ferromagnetism in Semihydrogenated Graphene Sheet. *Nano Lett.* **2009**, *9*, 3867–3870. [CrossRef]

25. Kharche, N.; Nayak, S.K. Quasiparticle Bandgap Engineering of Graphene and Graphone on Hexagonal Boron Nitride Substrate. *Nano Lett.* **2011**, *11*, 5274–5278. [CrossRef]

26. Barboza, A.P.M.; Guimaraes, M.H.D.; Massote, D.V.P.; Campos, L.C.; Neto, N.M.B.; Cancado, L.G.; Lacerda, R.G.; Chacham, H.; Mazzoni, M.S.C.; Neves, B.R.A. Room-Temperature Compression-Induced Diamondization of Few-Layer Graphene. *Adv. Mater.* **2011**, *23*, 3014–3017. [CrossRef]

27. Watanabe, N. Two Types of Graphite Fluorides, (CF)n and (C2F)n, and Discharge Characteristics and Mechanisms of Electrodes of (CF)n and (C2F)n in Lithium Batteries. *Solid State Ion.* **1980**, *1*, 87–110. [CrossRef]

28. Touhara, H.; Kadono, K.; Fujii, Y.; Watanabe, N. On the Structure of Graphite Fluoride. *Z. Für Anorg. Und Allg. Chem.* **1987**, *544*, 7–20. [CrossRef]

29. Novoselov, K.S. Nobel Lecture: Graphene: Materials in the Flatland. *Rev. Mod. Phys.* **2011**, *83*, 837–849. [CrossRef]

30. Rajasekaran, S.; Abild-Pedersen, F.; Ogasawara, H.; Nilsson, A.; Kaya, S. Interlayer Carbon Bond Formation Induced by Hydrogen Adsorption in Few-Layer Supported Graphene. *Phys. Rev. Lett.* **2013**, *111*. [CrossRef]

31. Piazza, F.; Monthioux, M.; Puech, P.; Gerber, I.C. Towards a Better Understanding of the Structure of Diamanoïds and Diamanoïd/Graphene Hybrids. *Carbon* **2020**, *156*, 234–241. [CrossRef]

32. McSkimin, H.J.; Andreatch, P. Elastic Moduli of Diamond as a Function of Pressure and Temperature. *J. Appl. Phys.* **1972**, *43*, 2944–2948. [CrossRef]

33. Wu, Y.-C.; Shao, J.-L.; Zheng, Z.; Zhan, H. Mechanical Properties of a Single-Layer Diamane under Tension and Bending. *J. Phys. Chem. C* **2020**. [CrossRef]

34. Zhu, L.; Hu, H.; Chen, Q.; Wang, S.; Wang, J.; Ding, F. Formation and Electronic Properties of Hydrogenated Few Layer Graphene. *Nanotechnology* **2011**, *22*, 185202. [CrossRef] [PubMed]

35. Kvashnin, A.G.; Chernozatonskii, L.A.; Yakobson, B.I.; Sorokin, P.B. Phase Diagram of Quasi-Two-Dimensional Carbon, From Graphene to Diamond. *Nano Lett.* **2014**, *14*, 676–681. [CrossRef]

36. Kvashnin, A.G.; Sorokin, P.B. Lonsdaleite Films with Nanometer Thickness. *J. Phys. Chem. Lett.* **2014**, *5*, 541–548. [CrossRef]

37. Piazza, F.; Gough, K.; Monthioux, M.; Puech, P.; Gerber, I.; Wiens, R.; Paredes, G.; Ozoria, C. Low Temperature, Pressureless Sp2 to Sp3 Transformation of Ultrathin, Crystalline Carbon Films. *Carbon* **2019**, *145*, 10–22. [CrossRef]

38. Piazza, F.; Cruz, K.; Monthioux, M.; Puech, P.; Gerber, I. Raman Evidence for the Successful Synthesis of Diamane. *Carbon* **2020**, *169*, 129–133. [CrossRef]

39. Chernozatonskii, L.A.; Mavrin, B.N.; Sorokin, P.B. Determination of Ultrathin Diamond Films by Raman Spectroscopy. *Phys. Status Solidi B* **2012**, *249*, 1550–1554. [CrossRef]

40. Bakharev, P.V.; Huang, M.; Saxena, M.; Lee, S.W.; Joo, S.H.; Park, S.O.; Dong, J.; Camacho-Mojica, D.C.; Jin, S.; Kwon, Y.; et al. Chemically Induced Transformation of Chemical Vapour Deposition Grown Bilayer Graphene into Fluorinated Single-Layer Diamond. *Nat. Nanotechnol.* **2020**, *15*, 59–66. [CrossRef]

41. Chen, X.; Dubois, M.; Radescu, S.; Rawal, A.; Zhao, C. Liquid-Phase Exfoliation of F-Diamane-Like Nanosheets. *Carbon* **2020**. [CrossRef]

42. Son, J.; Ryu, H.; Kwon, J.; Huang, S.; Yu, J.; Xu, J.; Watanabe, K.; Taniguchi, T.; Ji, E.; Lee, S.; et al. Tailoring Single- and Double-Sided Fluorination of Bilayer Graphene via Substrate Interactions. *Nano Lett.* **2020**. [CrossRef]

43. Cheng, T.; Liu, Z.; Liu, Z. High Elastic Moduli, Controllable Bandgap and Extraordinary Carrier Mobility in Single-Layer Diamond. *J. Mater. Chem. C* **2020**, *8*, 13819–13826. [CrossRef]

44. Chernozatonskii, L.A.; Demin, V.A.; Kvashnin, D.G. Ultrawide-Bandgap Moiré Diamanes Based on Bigraphenes with the Twist Angles Θ ∼30°. *Appl. Phys. Lett.* **2020**, *117*, 253104. [CrossRef]

45. Campanera, J.M.; Savini, G.; Suarez-Martinez, I.; Heggie, M.I. Density Functional Calculations on the Intricacies of Moiré Patterns on Graphite. *Phys. Rev. B* **2007**, *75*. [CrossRef]

46. Artyukhov, V.I.; Chernozatonskii, L.A. Structure and Layer Interaction in Carbon Monofluoride and Graphane: A Comparative Computational Study. *J. Phys. Chem. A* **2010**, *114*, 5389–5396. [CrossRef]

47. Li, H.; Duan, T.; Haldar, S.; Sanyal, B.; Eriksson, O.; Jafri, H.; Hajjar-Garreau, S.; Simon, L.; Leifer, K. Direct Writing of Lateral Fluorographene Nanopatterns with Tunable Bandgaps and Its Application in New Generation of Moiré Superlattice. *Appl. Phys. Rev.* **2020**, *7*, 011403. [CrossRef]

48. Chernozatonskii, L.A.; Katin, K.P.; Demin, V.A.; Maslov, M.M. Moiré Diamanes Based on the Hydrogenated or Fluorinated Twisted Bigraphene: The Features of Atomic and Electronic Structures, Raman and Infrared Spectra. *Appl. Surf. Sci.* **2021**, *537*, 148011. [CrossRef]

49. Wang, J.; Mu, X.; Wang, L.; Sun, M. Properties and Applications of New Superlattice: Twisted Bilayer Graphene. *Mater. Today Phys.* **2019**, *9*, 100099. [CrossRef]

50. Muniz, A.R.; Maroudas, D. Opening and Tuning of Band Gap by the Formation of Diamond Superlattices in Twisted Bilayer Graphene. *Phys. Rev. B* **2012**, *86*. [CrossRef]
51. Muniz, A.R.; Maroudas, D. Formation of Fullerene Superlattices by Interlayer Bonding in Twisted Bilayer Graphene. *J. Appl. Phys.* **2012**, *111*, 043513. [CrossRef]
52. Muniz, A.R.; Maroudas, D. Superlattices of Fluorinated Interlayer-Bonded Domains in Twisted Bilayer Graphene. *J. Phys. Chem. C* **2013**, *117*, 7315–7325. [CrossRef]
53. Machado, A.S.; Maroudas, D.; Muniz, A.R. Tunable Mechanical Properties of Diamond Superlattices Generated by Interlayer Bonding in Twisted Bilayer Graphene. *Appl. Phys. Lett.* **2013**, *103*, 013113. [CrossRef]
54. Muniz, A.R.; Machado, A.S.; Maroudas, D. Mechanical Behavior of Interlayer-Bonded Nanostructures Obtained from Bilayer Graphene. *Carbon* **2015**, *81*, 663–677. [CrossRef]
55. Chen, M.; Muniz, A.R.; Maroudas, D. Formation and Mechanical Behavior of Nanocomposite Superstructures from Interlayer Bonding in Twisted Bilayer Graphene. *ACS Appl. Mater. Interfaces* **2018**. [CrossRef]
56. Cellini, F.; Lavini, F.; Cao, T.; de Heer, W.; Berger, C.; Bongiorno, A.; Riedo, E. Epitaxial Two-Layer Graphene under Pressure: Diamene Stiffer than Diamond. *FlatChem* **2018**, *10*, 8–13. [CrossRef]
57. Ke, F.; Zhang, L.; Chen, Y.; Yin, K.; Wang, C.; Tzeng, Y.-K.; Lin, Y.; Dong, H.; Liu, Z.; Tse, J.S.; et al. Synthesis of Atomically Thin Hexagonal Diamond with Compression. *Nano Lett.* **2020**, *20*, 5916–5921. [CrossRef]
58. Paul, S.; Momeni, K.; Levitas, V.I. Shear-Induced Diamondization of Multilayer Graphene Structures: A Computational Study. *Carbon* **2020**, *167*, 140–147. [CrossRef]